Experimental Assessment of 'subgrid' scale Probability Density Function Models for Large Eddy Simulation

Yannis Hardalupas [1,*], Nikolaos Soulopoulos [1], Viacheslav Stetsyuk [1] and Alex M. K. P. Taylor [1]

1: Imperial College London, Department of Mechanical Engineering, South Kensington Campus, London, UK
* corresponding author: y.hardalupas@imperial.ac.uk

Abstract Filtered density functions (FDFs) of mixture fraction are quantified by analyzing experimental data obtained from two-dimensional planar laser-induced fluorescence scalar measurements in the isothermal swirling flow of a combustor operating at a Reynolds number of 28,662 for three different swirl numbers (0.3, 0.58 and 1.07). Two-dimensional filtering using a box filter was performed on the measured scalar to obtain the filtered variables used for presumed β-FDF and top-hat FDF for Large Eddy Simulations (LES). A dependant variable from the measured scalar, which was a pre-computed temperature, was integrated over the experimentally obtained FDF as well as over the presumed beta or top-hat FDFs and a relative error in temperature prediction was calculated. The experimentally measured FDFs depended on swirl numbers and axial and radial positions in the flow. The FDFs were unimodal in the regions of low variance and bimodal in the regions of high variance. The influence of the filter spatial dimension on the measured FDF was evaluated and consequences for Subgrid modeling for LES discussed.

1. Introduction

In Large Eddy Simulations (LES) of turbulent reacting flows, spatially-averaged versions of the equations describing motion and chemical reaction are usually solved on a grid, which is 'coarse' relative to the smallest scales of the fluid motion. The effects of the smallest scales are modeled in order to 'close' the LES equations. Models of the LES of combusting flows rely on the probability density function (PDF) of the sub-grid scale (SGS) species mass fractions, where 'sub-grid' refers to motions that are smaller than the computational grid size. The filtered quantity f (velocity, mixture fraction etc.) in physical space is simply defined as a convolution of non-filtered field with a function or convolution kernel as.

$$\overline{f}(x) = \int f(x')G(x-x')dx' \tag{1}$$

In a non-premixed flame, fuel and oxidizer diffuse into the reaction zone where they undergo chemical reaction and are converted to combustion products. In flames that are near equilibrium the reaction rate is much faster than the diffusion rate, which is governed by the mixture fraction gradients. In turbulent reacting flows, the flame is stretched and wrinkled due to turbulent motions so that the temperature, mixture fraction and species gradients increase. These gradients increase the diffusion out of the reaction zone and the local non-equilibrium increases. If the assumption of local equilibrium is valid then, *e.g.* a laminar flamelet model can be used to model such regime. The flamelet approach can be seen as a way of decoupling chemistry from the CFD solver. In adiabatic systems flame temperature, species mass fractions etc. are parameters of the mixture fraction and the scalar dissipation rate that can be pre-computed. Therefore, it is possible to obtain so called look up tables with values of temperature, species mass fractions etc. as a function of scalar dissipation rate, the mixture fraction or both. Since in LES only filtered values of the flow field are known, it is impossible to integrate the look-up tables in order to obtain the

temperature and the species mass fractions because no "subgrid" distribution is known.

A general approach to integrate the look-up flamelet tables over the subgrid scales in computational modeling is based on the solution of a transport equation for the FDF, which is similar to the transport equation for the Reynolds Averaged Navier Stokes (RANS) PDF approach. However, the most simplified and commonly used approach is based on presumed filtered density functions, which are usually approximated to be β or top-hat functions and parameterized by the first two moments of the mixture fraction, namely the filtered mixture fraction and its variance. The success of transported PDF methods (Pope, 1985) in the RANS context promoted the development of the transported FDF concept in the LES context. Transported FDF methods have been developed for instance by Gao & O'Brien (1993), Colucci et al. (1998), Sheikhi et al. (2003), Raman et al. (2006). The validity and applicability of presumed FDF methods were also investigated by several authors using DNS data of non-premixed reacting flows (Cook & Riley 1994; Jimenez et al. 2000; Floyd et al. 2009). The results confirmed that the presumed FDF methods, based on beta-function, provided a good estimate for the FDF of the mixture fraction. However, Tong (2001) and Tong et al. (2005) showed that the 'real' FDF can substantially deviate from the beta-function approximation.

If an assumption of linearity within the LES cells is made, the FDF can also be approximated by so called top-hat function (Borghi and Moreau, 1977). The top-hat function, spanning from minimum mixture fraction value z_a to maximum value z_b, and the beta function are defined as:

$$\Pi_l\left(\overline{z},\overline{z}^{"2}\right)=\frac{1}{z_b-z_a};\ z_a=\overline{z}-\frac{l}{2};\ z_b=\overline{z}+\frac{l}{2};\ l=\sqrt{12\overline{z}^{"2}} \tag{2}$$

$$B_z\left(\overline{z},\overline{z}^{"2}\right)=\frac{z^{a-1}\left(1-z\right)^{b-1}}{\int_0^1 z^{a-1}\left(1-z\right)^{b-1}dz};\ a=\overline{z}\left(\frac{\overline{z}\left(1-\overline{z}\right)}{\overline{z}^{"2}}-1\right);\ b=\left(1-\overline{z}\right)\left(\frac{\overline{z}\left(1-\overline{z}\right)}{\overline{z}^{"2}}-1\right) \tag{3}$$

where the parameters of the above equations are defined in Section 6 of the paper.

The filtered mixture fraction is determined by the solution of the transport equations and its variance is usually modeled by different algebraic models. If the FDF is known then all dependant variables can be computed. For instance, if chemistry is assumed to be infinitely fast then local equilibrium is reached and mass fractions, a reaction rate or a temperature are functions of mixture fraction z only. In this case all dependant variables (e.g. a temperature) can be computed. The concept of the FDF can also be extended to finite-rate chemistry. In this case, the FDF is a joint function of mixture fraction and its scalar dissipation rate, but this is beyond the scope of the present work. Generally, the FDF can be constructed from any sub-filter scalar variable that is obtained from experiments as follows. At a given spatial location, a box filter of known size is applied and the scalar values, *e.g.* of mixture fraction, are extracted and binned into 10-15 bins, which then can easily be converted into the FDF by counting frequencies and dividing them by a relative bin width (bin width times the cardinality of a set). Mathematically the filtered density function of a scalar f is given according to the following formula (Tong, 2001):

$$f_\phi(\hat{\phi};x,t)=\int\delta\left[\phi\left(x,t\right)-\hat{\phi}\right]G\left(x-x^{'}\right)dx \tag{4}$$

The shape of the filtered density function may change the resolved dependant variables such as temperature, species mass fraction, density etc. In this work the resolved dependant variable was chosen to be the resolved temperature due to the interest of this work to models for turbulent reacting flows. The beta and top-hat functions were parameterized by the first two moments of

mixture fraction, i.e. resolved mean and its variance. The resolved dependant mean Temperature can be computed then according to the following formulas:

$$\overline{T}_{f_z} = \int_0^1 T(z) f_z\left(x,t\right) dz \tag{5}$$

$$\overline{T}_{\beta} = \int_0^1 T(z) B_z\left(\overline{z}, \overline{z}^{"2}\right) dz \tag{6}$$

$$\overline{T}_{\Pi_l} = \int_0^1 T(z) \Pi_l\left(\overline{z}, \overline{z}^{"2}\right) dz \tag{7}$$

The 'subgrid' scale variance, used in the presumed FDF modeling approach, was computed according to the following formula:

$$\overline{z}^{"2} = \int \left\{ z(x) - \overline{z}(x) \right\}^2 G(x - x^{'}) dx \tag{8}$$

In order to compute the resolved mean temperature from the measured mixture fraction, the relationship between temperature and mixture fraction must be known. This assumption is valid in the case of fast chemistry and is used in this work to convert the measured scalar concentration into temperature. In the case of finite chemistry a similar approach to compute the resolved mean temperature can be adopted even though it is not considered here. The relationship between flame temperature and mixture fraction was computed by using the commercial software CHEMKIN-Pro©. CHEMKIN-Pro© is made of different FORTRAN subroutines that allow modeling of different reacting systems under different operating conditions. The software uses detailed chemical mechanism to compute chemically reacting flows, which is by default the GRI-3.0. However, in this work the San Diego mechanism, thermodynamic database and the transport database were chosen. This data were published by University of California at San Diego (UCSD). In the San Diego mechanism, the number of species and reaction is kept to the appropriate minimum needed to accurately describe the modeled system, thus minimizing the uncertainties from the chemical reaction rate parameters. This approach significantly differs from other data sets, for example GRI-3.0. The other data sets attempt to include all potentially relevant elementary steps that can lead to the uncertainties, especially when large number of steps is used. A subroutine (OPPDIF) was used to compute the flame temperature of methane/air diffusion flame at atmospheric pressure and temperature. OPPDIF simulates the flame structure for axisymmetric or planar diffusion flames between two opposed flow nozzles. This procedure is equivalent to generating laminar-flamelet libraries to be used with CFD codes. The OPPDIF subroutine is based on a model that was originally proposed by Kee et al. (1988), where the detailed derivation of the governing equations that are used in OPPDIF can also be found and are not presented here.

The remaining paper is structured as follows. Section 2 describes the swirling air flow burner and the optical instrumentation used to measure the scalar, which is then converted to the temperature according to the explanation provided above. Section 3 describes the results and discusses the findings in terms of the differences between the measurements and the results from the presumed FDF approaches used in LES. The paper ends with a summary of the main conclusions.

2. Experimental setup

The burner used in this study is shown in Figure 1 and was based on the design of Dixon et al. (1983) and replicated in the work of Milosavljevic (1993). The burner comprised two concentric pipes with the annulus supplying air and the central pipe delivering air seeded with acetone vapor, which is the measured scalar quantity. The central pipe had an inner diameter D_f of 15mm

and an outer diameter of 18 mm, was 0.75m long and was located concentrically in the outer pipe of inner diameter, *D*, 50.8 mm and length downstream of the swirl chamber of 264mm. The annular air stream was divided into two separately metered streams. One (`tangential air') passed through a static Swirler containing six tangential slots to impart angular momentum. The static Swirler was located in a plenum chamber in which the Swirling air was combined with the second stream, which delivered 'axial air'. Metal plates were installed in the axial and tangential air sections of the plenum chamber to ensure that the axial and tangential air streams were distributed uniformly upstream of the inlets into the annular air supply stream of the burner, where they were combined to control the strength of Swirl at the burner exit. The tangential and axial air flowrates were metered by flowmeters after correction to atmospheric pressure and temperature. The axial direction, parallel to the flow propagation, was denoted as “y” and the radial direction, perpendicular to the main direction of the flow, as “x”. The swirl number is defined as follows:

$$S = \frac{2G_\Theta}{G_Z D} \tag{9}$$

where S is the Swirl number, G_Θ is the axial flux of angular momentum and G_z is the axial flux of axial momentum and are determined below as:

$$G_\Theta = 2\pi\rho \int_{r=r_i}^{R} WrUrdr$$

$$G_Z = 2\pi\rho \int_{r=r_i}^{R} UUrdr$$

where U and W are the axial and tangential velocity components and r_i and R the radius of the inner and outer pipe respectively.

The swirl number of the secondary air was calculated in the work of Milosavljevic (1993) using measured axial and tangential velocity profiles with a laser Doppler anemometer at 0.04D downstream of the exit plane of the burner and its value is presented in Table 1 along with operating conditions used during experiments.

Table 1: Operating conditions

S	V axial, l/min	V swirl, l/min	V fuel, l/min	U fuel, m/s	U air, m/s	Re, air	Re, fuel
1.07	150	750	40	3.77	8.46	28662	3770
0.58	350	550	40	3.77	8.46	28662	3770
0.30	500	400	40	3.77	8.46	28662	3770

Note: U – denotes velocity, S –swirl number and V- volumetric flow rate in liters per minute

A class-IV high power Q-switched Nd:YAG frequency-quadrupled 266nm laser from Continuum Inc., USA was used to excite the acetone vapor fluorescence. The laser beam was produced at the fundamental wavelength of 1064nm (1050mJ) and passed through frequency doubler to produce 532nm (green light, 455mJ) then passed through a fourth harmonic generator in order to produce 266nm (： 120mJ) at the exit port of the laser. The laser pulse width was in the range of 5： 7 ns at Full Width at Half Maximum (FWHM). A single diachronic mirror was used to decrease the amount of 532nm light reaching the burner and to steer the laser beam from the laser exit port towards the experimental setup and sheet forming optics. The sheet forming optics consisted of a single cylindrical positive lens with focal length of 300mm. The lens was used to focus the laser beam into a thin waist, with focal point located at the axis of symmetry of the flow. The average laser energy at the test section was 70mJ/pulse. Actual laser energy fluctuated during experiments from pulse to pulse and was equal to 65÷70 mJ/pulse.

Instantaneous corrections of the sheet profile intensity variations were not performed. The mean laser sheet profile was acquired and was used in the image correction procedure.

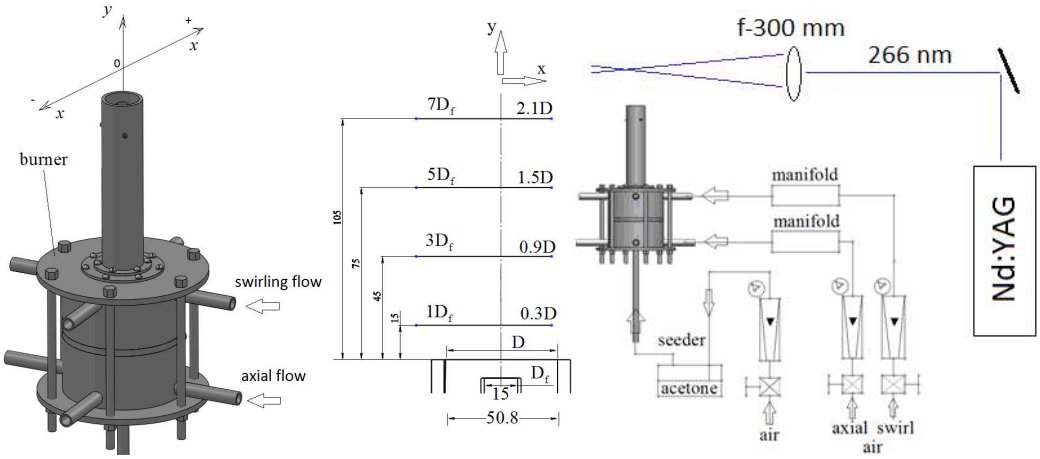

Figure 1: Atmospheric burner used for scalar measurements under isothermal conditions, laser sheet locations for optical measurements and optical instrumentation arrangement.

A double frame Charge Couple Device (CCD) (Imager Intense) camera from LaVision Inc. was used in this work. This camera was equipped with a Nikkor lens with focal length $f_l = 50\,\text{mm}$ and f#1.4 (where f# is the f-number). A 13mm extension ring was also used after the camera lens for tighter focusing. A BG3 bandpass Schott filter was used in front of camera lens in order to block any remaining 532nm light that might interfere with the acquired signal. Any scattered 266nm UV light that might come from the test volume was blocked by the glass material of the camera lens. The array size of the CCD camera was 1376 x 1040 pixels and the pixel size was $6.45\,\mu\text{m}$. The optical magnification was determined by using a calibration target plate and was found to be 0.0263 mm/pixel. The laser sheet thickness was determined to be 0.15mm. Both the laser and the CCD camera were electronically controlled from software package DaVis 7.2, provided by LaVision Inc. USA, installed on a computer running Windows XP. The computer, which ran the LaVision© software package (version 7.2) was used for all aspects of the experiment, including tuning the system, calibration and acquiring the experimental data. Data communication lines from the laser and camera were input to the computer. Post-processing was performed by using commercial software package MATLAB© R2009b in order to quantify the acetone vapor concentration. This was converted to Temperature using the approach described in Section 1.

The FDFs were calculated from the instantaneous imaging for two box filter sizes, namely 0.3 and 1.0mm. The ratios of the filter size to turbulent dissipative scales are summarized in Table 2. Tong et al. (2007) pointed out that filter sizes should be significantly larger compared to the dissipative scales to ensure that the results are relevant to LES. However, it is not yet clear what the optimal ratio of typical LES filter size to dissipative scales is. As noted by Meyers et al. (2008), "a good LES is almost DNS". In general, the LES results should be in better agreement with DNS if the LES filter size Δ is chosen to be as close as possible to Kolmogorov scale and when $\Delta < \eta$ the turbulence is fully resolved. Larger filter size, i.e. larger than 1.0mm in the current flow, was not used because the FDF was found to be bimodal even at this filter size.

Table 2: Filter to dissipative scale ratio. Two box filters were used, i.e. 0.3 and 1.0mm.

S	$\eta, \mu m$	$\lambda_B, \mu m$	$\Delta/\eta\|_{\Delta=0.3}$	$\Delta/\lambda_B\|_{\Delta=0.3}$	$\Delta/\eta\|_{\Delta=1.0}$	$\Delta/\lambda_B\|_{\Delta=1.0}$
0.3	246	243	1.219	1.234	4.065	4.115
0.58	184	167	1.630	1.796	5.435	5.988
1.07	107	97	2.804	3.093	9.346	10.309

The process of calculation of the FDF from two-dimensional data involved binning the scalar data in 10-15 equally spaced bins. The discrete values of scalar data that fell in each bin were counted so that frequency of occurrence was calculated. The value of FDF was then obtained by normalizing estimated frequencies by the corresponding bin width and the total number of samples in all bins. The total number of samples depends on the box filter sizes. For instance, if the box filter is 1mm, which corresponds to 38 pixels on the images, then the total number of samples will be 38x38. The filtered mixture fraction field in physical space was simply obtained as a convolution of non-filtered field with a box filter according to Eqn. (1). The 'subgrid' scale variance, which was used in the presumed FDFs, was computed according to Eqn. (8) as follows. A box filter was applied, *e.g.* 1.0mm, which occupied an area of 38 pixels by 38 pixels on the instantaneous images of scalar concentration. Then, by placing this spatial filter at one location of an instantaneous image the average values were computed as the sum of all samples within the filter box divided by a number of samples in the bin. This mean value, which is defined as resolved mean, was assigned at the center of the box filter and then the filter was translated by 1 pixel increment steps along the instantaneous image, thus performing the filtering procedure. The 'subgrid' scale variance vas computed by subtracting the mean (computed from the box filter) of each instantaneous mixture fraction sample that was within the filter area. The resulting values were squared, averaged and assigned to the centre of the filter box.

Nine different spatial locations at each laser sheet axial position were studied. The specific positions are shown in Figure 2 where the effects of swirl are to be examined as a function of degree of mixing. The six spatial locations were chosen to be within the shear layer, where highly segregated flow within the filter is observed, and three at the burner centerline, where nearly homogeneous flow field is expected. In fact, windows 1, 4, 7 and 3, 6, 9 demonstrate similar trends and were chosen to decrease possible random errors.

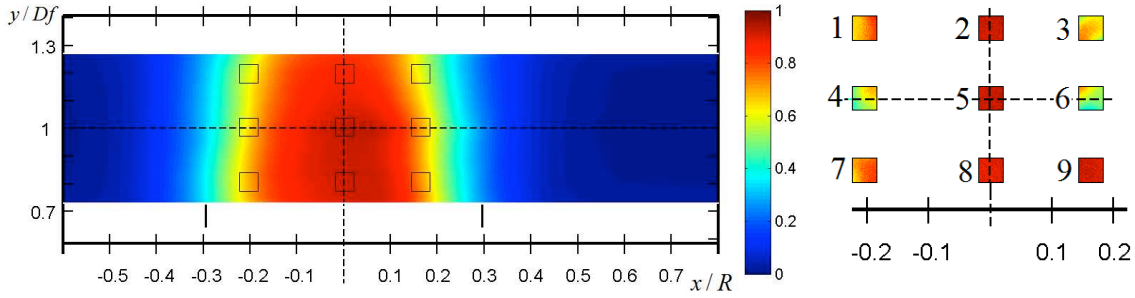

Figure 2: Time-averaged mixture fraction distribution (computed from 1500 realizations) for axial distance from the burner exit of $1D_f$ and S=0.3 and selected spatial locations used to compute the FDFs. The spatial location used to compute the FDF was chosen within the shear layer and the burner centerline, which is denoted as vertical dashed line. The figure is presented on non-dimensional coordinates, namely dimensionless centerline (axial) positions and dimensionless radial positions. The radial distance from the centreline was normalised by the burner radius R and the axial distance from the burner exit was normalised by the central pipe diameter D_f.

3. Results and discussion

Examples of measured instantaneous (before any spatial filtering) mixture fraction spatial distributions at different axial distances from the burner exit, *i.e.* $7D_f$, $5D_f$, $3D_f$, $1D_f$ (from top to bottom respectively) and S=0.58 are shown in Figure 3. The diameter of the central pipe is D_f=15mm and the small short vertical lines at ±0.3 x/R denote its position. The vertical dashed line denotes the burner centreline. As expected the mixture fraction is maximum close to the centreline and reduces with radial distance, since the scalar concentration is lower at the edge of the central jet. The mixing process, which is enhanced by the presence of swirl, ensures that the scalar is well mixed away from the burner exit. Therefore, the spatial variation of the mixture fraction is small at $7D_f$, which results in small 'subgrid' scale variance after filtering.

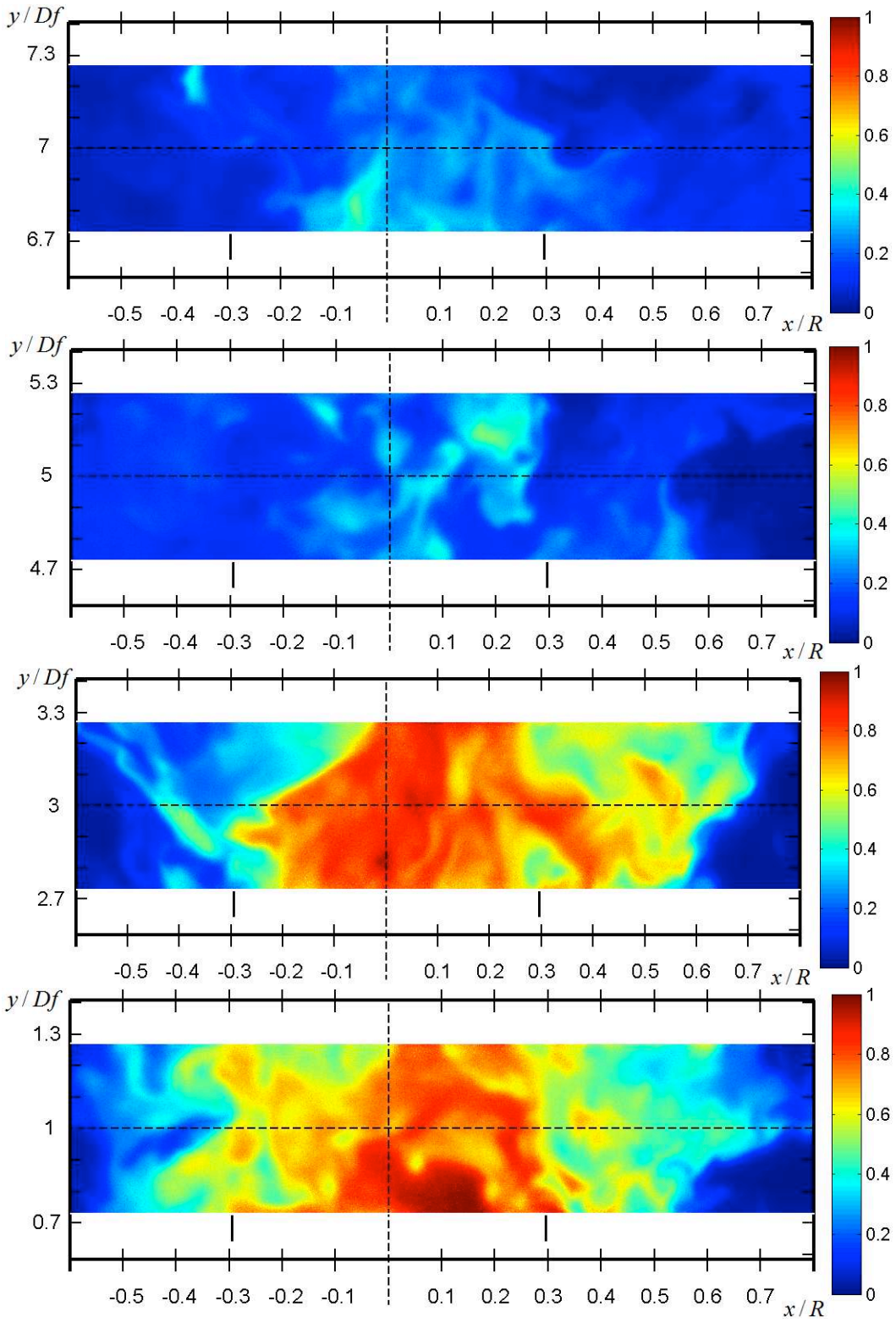

Figure 3: Examples of measured instantaneous mixture fraction fields at different axial distances from the burner exit, i.e. $7D_f$, $5D_f$, $3D_f$, $1D_f$ (from top to bottom) and S=0.58. At $7D_f$ the variation of the mixture fraction is small, which results in small subgrid scale variance. This in fact will indicate that at this location the FDF is bimodal. Vertical dashed line denotes the burner centerline. D_f=15mm, R = 25.4mm. Small short vertical lines at ±0.3 x/R denote the position of the central pipe.

Figure 4 shows an example of two measured FDFs of mixture fraction estimated from the presented single realization (instantaneous scalar field) at window 1 of Figure 2 for two different spatial filter sizes of 1.0mm and 0.3mm (shown as two black boxes on the figure) at $1D_f$ and S=0.3. This figure demonstrates the qualitative change of the shape of the FDF as a function of box filter size. It is clear that for large size filter of 1.0mm, the FDF is bimodal and it becomes unimodal when the size of the spatial filter is reduced to 0.3mm. In addition, if the box filter overlaps with an area that demonstrates steep gradient of mixture fraction, the FDF can be bimodal. In contrast, if the box filter is chosen to be small enough (i.e. close to Kolmogorov or Batchelor scales) then it resolves homogeneous mixture fraction regions, in which the SGS variance is small. Due to space limits, the findings for other window positions are not supported by graphical representations. However, at window 2 and for S=0, the FDF is approaching a delta function for the both box filter sizes, i.e. 0.3 and 1.0mm, due to the fact that the mixture fraction is always one at that region.

Similar results can be observed at window 2 (as well as at windows 5 and 8) for S=0.3, because mixing is good and the field is nearly homogeneous. It should be noted that windows 1, 4 and 7 'mirror' the behaviour of the FDF in windows 3, 6 and 9. In fact, all nine spatial locations in the flow were considered to ensure that the FDF behaviour is not affected by the data processing method or random errors.

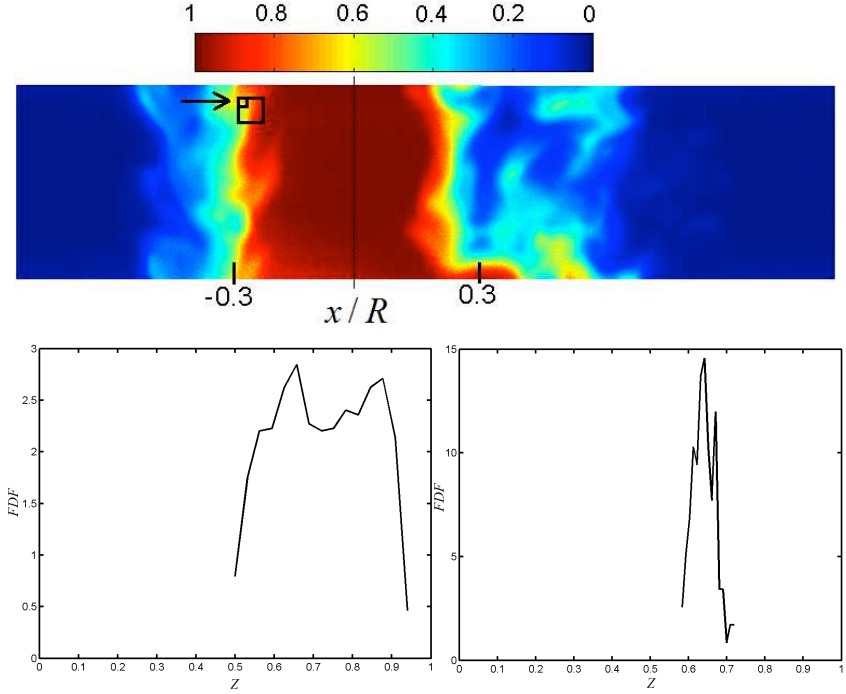

Figure 4: Example of two measured FDFs estimated from the presented single realization (instantaneous scalar field) at window 1 for two different spatial filter sizes of 1.0mm and 0.3mm (shown as two black boxes on the figure) at $1D_f$ and S=0.3. Vertical scale is not provided on the instantaneous scalar image because the figure aims to illustrate the qualitative change of the shape of the FDF as a function of box filter size.

Several measured FDFs for different large and small SGS variances of mixture fraction are presented in Figures 5 and 6 as a function of axial position in the flow and flow swirl number. It should be noted that the FDF computations are presented here for one location only (at window 1 of Figure 2) due to limitations on the length of the paper. The conserved scalar FDFs exhibit two clearly visible regimes, which are denoted as "homogeneous" (Figure 6) and "non-homogeneous" (Figure 5). The term "homogeneous" is related to the unimodal distribution of the FDF, while the term "non-homogeneous" is related to bimodal distribution of the FDF.

The two different shapes of FDF distributions were observed in flow regions where high and low mixture fraction segregations were present (see Figures 5 and 6). Bimodal distributions

occur for both fuel-rich and fuel-lean values of mixture fraction, when SGS variance is large. Unimodal distributions are found when SGS variance is small. When SGS variance decreases, the corresponding beta-FDF and top-hat functions are close to each other and in a limiting case become delta-functions.

Figures 5 and 6 also present the corresponding shapes of presumed β-FDF and top-hat FDF, constructed from the resolved mean and the measured SGS variance (according to Eqn. 1 and 8). Figure 5 presents the FDF measurements from window 1 at $5D_f$, $3D_f$, $1D_f$ for two flow regimes with S=0 (axial jet without coflow of air) and S=0.3 and for box filter size of 1.0mm. Figure 6 presents measurements at the same axial positions for S=0.58 and S=1.07. Figure 5 illustrates that when flow is segregated within the filter volume the FDF becomes bimodal, which is due to non-mixed regime. On the other hand in Figure 6 unimodal distributions are clearly observed.

The effect of swirl number can be seen in Figure 5 (for S=0 and S=0.3) and Figure 6 (for S=0.58 and S=1.07) as an increase in the level of mixing, which increases homogeneity of the flow field. That is, at the same spatial location in the flow, but for different swirl numbers the FDF can be either bimodal or unimodal. The results confirm that higher swirl numbers increase unimodality, especially at large axial distances, i.e. $5D_f$ and $7D_f$. A unimodal distribution was observed at all nine spatial locations for 1500 instantaneous realizations at $7D_f$ and swirl number of 1.07 due to small subgrid scale variance. This is also consistent with Tong et al. (2007), who measured the conditional filtered mass density functions (FMDF) in reacting flows. They pointed out that the conditional FMDF was found to be unimodal, and not far from Gaussian, when the subgrid scale variance was small. The SGS variance represents how far mixture fraction values can deviate from the mean and hence the SGS variance can characterize the rate and the level of mixing within one LES cell. For larger variance, the FMDF was found to be bimodal. Larger subgrid scale variance indicates that fuel and air are essentially segregated within filter volume. The SGS variance depends on the LES filter width and unmixedness and therefore is directly related to the local scalar mixing. It should be noted that the actual spatial resolution of the mixture fraction and the actual box filter size are larger than the nominal values due to optical system distortions and imperfections. Extra pixels should be added to each spatial filter to compensate for imperfections of the optical system. It is generally assumed that the difference between nominal and actual filter size will make little discrepancy in the FDF.

The integrated resolved mean temperature obtained from CHEMKIN solution is summarized in Table 3. The table describes several temperature integrations as the dependant variable for several SGS variances. The temperature integration was performed for several SGS variances, so that large and small variances were considered. For large variance and hence high bimodality, the difference between the temperature computed with actual measured FDF and the beta-FDF was ranging from 5% to 0.2%. In most cases, the difference in the resolved temperature calculation computed by different presumed FDFs is not significant (less or equal to 1%). This implies than the actual source of error in LES computations may be due to subgrid variance models and not due to presumed FDF approaches. This is also consistent with the conclusions from the LES calculations of Floyd et al. (2009). However, in some cases the difference can be as high as 18% for the top-hat FDF. On the other hand, there is no evidence that large SGS variance can introduce significant errors because there is no direct correlation between the measured SGS variance and the computational error, computed from the dependant variables. This is in fact applied to beta-FDF, where large temperature error can be found for smaller SGS variance and in turn smaller errors can be found for larger SGS variance. The top-hat FDF can potentially introduce significant errors, especially when large SGS variance is observed. It should be pointed out that the beta-FDF function can provide an adequate approximation of the 'true' FDF of the mixture fraction. Even in case of large variances, it does not automatically imply that bimodality can be the source of error. It also should be pointed out that when SGS variance is small, the beta-FDF and the relatively simple top-hat FDF are close to each other.

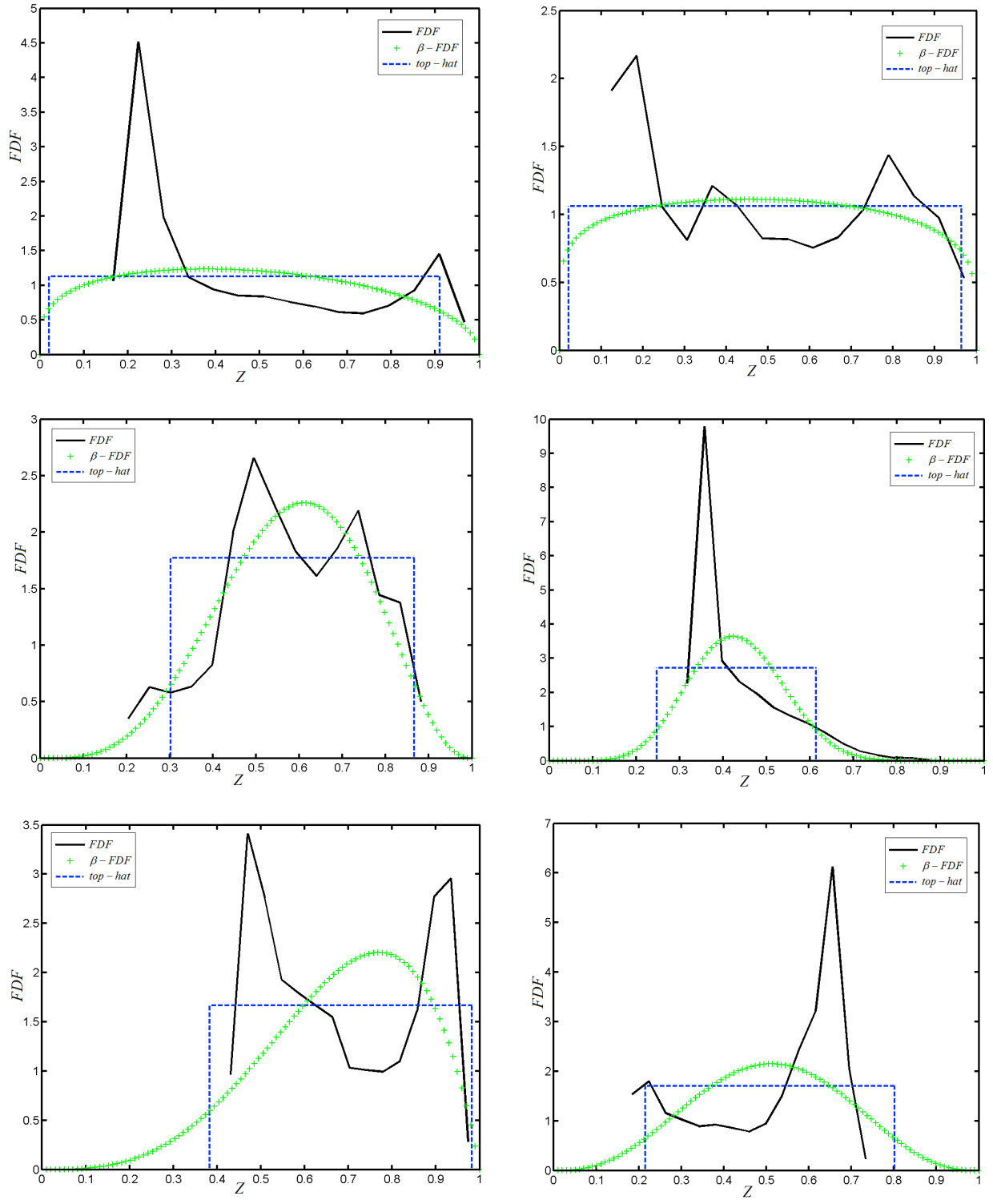

Figure 5: Measured FDFs computed from single realizations at window 1 of Figure 2 plotted for different large variances; β-FDF and top-hat FDF are shown as green dashed and blue dashed lines. The bimodal shape indicates that the fuel and air are essentially segregated within the box filter volume indicating non-mixed regime. The segregation can be due to insufficient mixing or due to the filter size, i.e. for the same spatial location two different filter sizes produce different FDFs. It should be noted that the values of the FDF printed along y-axis are not the same. From top to bottom are shown the FDFs at $1D_f$, $3D_f$ and $5D_f$, where on the left is the flow for S=0 (axial), on the right is the flow for S=0.3 for box filter size of 1.0mm.

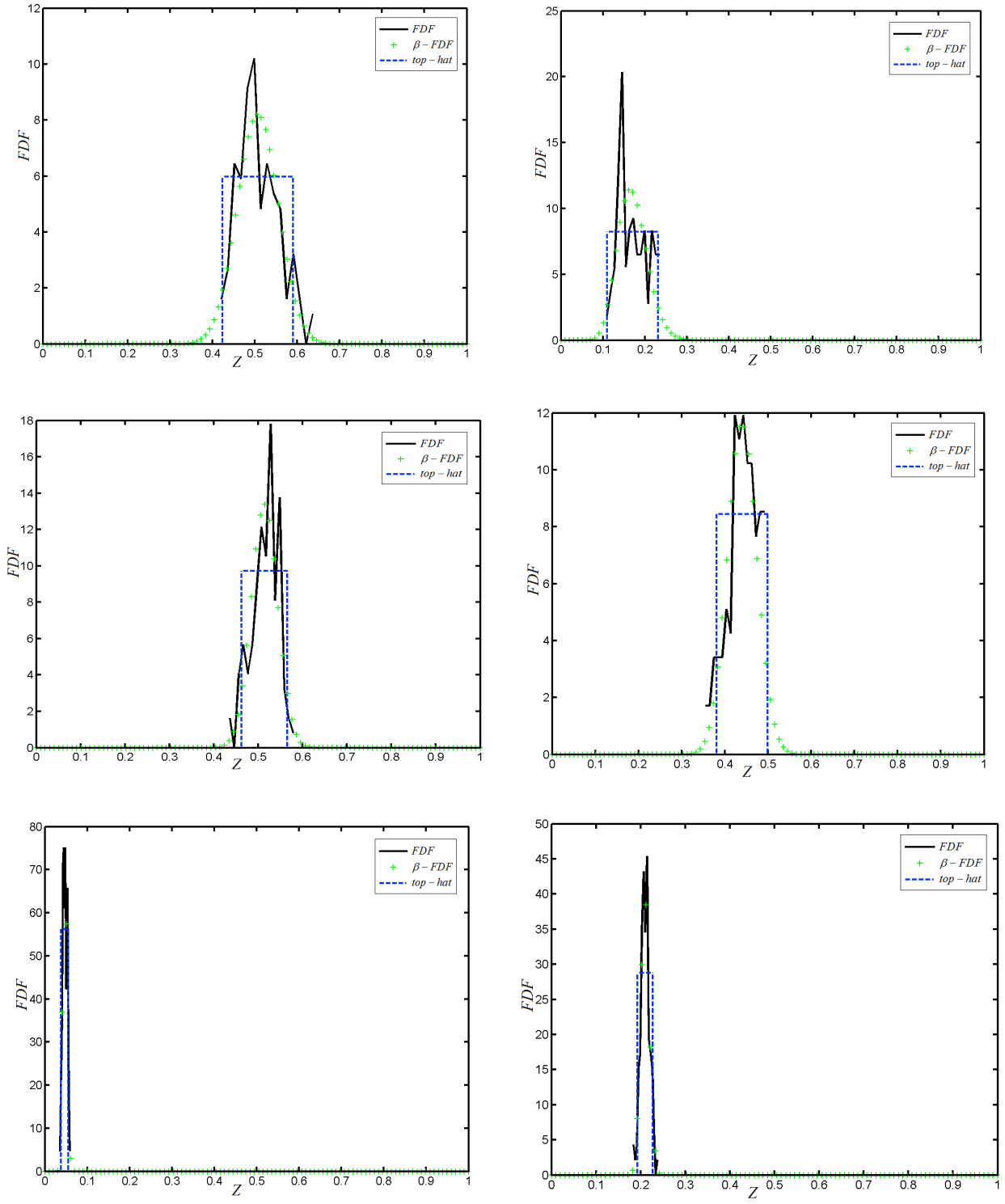

Figure 6: Measured FDFs from instantaneous realization plotted for different small variances and box filter of 1.0mm; β - and top-hat FDFs are shown as green dashed and blue dashed lines respectively. The unimodal shape indicates that the subgrid scale variance is small, which is due to either well-mixed regime or due to non-mixed regime as, for example, in a potential core of a jet. It should be noted that the values of the FDF printed along y-axis are not the same. From top to bottom are shown for $1D_f$, $3D_f$ and $5D_f$, where left column corresponds to S=1.07 and left to S=0.58.

Table 3: Resolved mean temperature integrated over the measured and presumed beta and top-hat FDFs

$\bar{z}$	$\bar{z}^{"2}$	$\bar{T}_{f_z},K$	$\bar{T}_{\beta},K$	$\bar{T}_{\Pi_l},K$	$\Delta_{\beta},\%$	$\Delta_{\Pi_l},\%$
0.465	*0.0659*	*1017*	*1019*	*826*	*0.197*	*18.780*
0.584	*0.0265*	*783*	*790*	*841*	*0.894*	*7.407*
0.682	*0.0299*	*654*	*687*	*668*	*5,046*	*2.141*
0.493	*0.0741*	*993*	*978*	*807*	*1.510*	*18.731*
0.430	*0.0112*	*989*	*1040*	*1003*	*5.157*	*1.415*
0.507	*0.0023*	*852*	*863*	*862*	*1.290*	*1.174*
0.514	*0.00088*	*842*	*851*	*845*	*1.069*	*0.356*
0.047	*0.000026*	*1816*	*1837*	*1802*	*1.156*	*0.771*
0.171	*0.0012*	*1594*	*1611*	*1604*	*1.066*	*0.627*
0.440	*0.0012*	*956*	*966*	*961*	*1.046*	*1.046*
0.210	*0.0001*	*1471*	*1486*	*1472*	*1.020*	*0.021*

Note: Computational error is calculated according to the following formulas

$\Delta_{\beta} = \left| \frac{\bar{T}_{f_z} - \bar{T}_{\beta}}{\bar{T}_{f_z}} \right| \cdot 100\%$ (beta-FDF); $\Delta_{\Pi_l} = \left| \frac{\bar{T}_{f_z} - \bar{T}_{\Pi_l}}{\bar{T}_{f_z}} \right| \cdot 100\%$ (top-hat FDF)

4. Conclusions

This paper presents an attempt to analyze the properties of the filtered density function of mixture fraction, measured in an isothermal swirling flow after filtering at two different scales, and compare it with assumed beta-FDF and top-hat FDF, which are commonly used in LES computations. The experiments were carried out on the swirling isothermal air flows seeded with acetone and confirmed the theory that the shape of the FDF was highly dependent on the sub-grid scale variance. It was proven that unimodality or bimodality can be observed at the same spatial location for different spatial filter sizes, different axial locations and different swirl numbers. On the other hand a direct correlation between the FDF shape and dependant variable integration error was not found. This means that even when FDF is highly bimodal, the presumed top-hat or β-FDF integrate the resolved mean temperature correctly. However, in some cases with small SGS variance, the temperature might not be integrated correctly either by β-FDF or top-hat FDF. Therefore, the main error that may arise in LES simulations is an adequate prediction of the SGS variance. Nevertheless, the concept of the filtered density function applied to LES computations is still an adequate choice for solving combustion problems given that the SGS variance is modeled accurately.

5. Acknowledgment

This work was partially supported by Alan Howard scholarship for Energy Futures.

6. Nomenclature

$\bar{z}$ – Mixture fraction (instantaneous unfiltered)
$\bar{z}^{"2}$ – Mean value of resolved Mixture fraction
$\bar{T}_{f_z}$ – Variance of resolved mixture fraction
$\bar{T}_{\beta}$ – Resolved mean temperature computed by integration of measured FDF, [K]
$\bar{T}_{\Pi_l}$ – Resolved mean temperature computed by integration of presumed β-FDF, [K]
Δ_{Π_l} –Resolved mean temperature computed by integration of presumed top-hat FDF, [K]
Δ_{β} – Integration temperature computational error between β-FDF and the measured FDF, [%]
Δ_{Π_l} –Integration temperature comp. error between top-hat FDF and the measured FDF, [%]
f_z – Measured FDF
B_z – Presumed β-FDF
Π_l – Presumed top-hat FDF
η – Kolmogorov length scale, [μm]
λ_B – Batchelor length scale, [μm]
Δ – Box filter width, [mm]
S – Swirl number

7. References

1. J. Floyd, A. M. Kempf, A. Kronenburg and R. H. Ram. A simple model for the filtered density function for passive scalar combustion LES. Combustion Theory and Modelling, 13:4, pp.559-588, 2009.
2. A. Kempf, W. Malalasekera, K. K. J. Ranga-Dinesh and O. Stein. Large eddy simulations of swirling non-premixed flames with flamelet models: A comparison of numerical methods. Flow Turbulence Combust, 2008.
3. W. Kollman and J. Janicka. The probability density function of a passive scalar in turbulent shear flows. Physics of Fluids, 25 (10), pp.1755-1769, 1982.
4. J. Meyers et al. (eds). Quality and Reliability of Large-Eddy Simulations, © Springer Science+Business Media B.V. 2008. p.93.
5. V.D. Milosavljevic. Natural gas, kerosene and pulverized fuel fired swirl burners. PhD thesis. University of London, July 1993.
6. S. B. Pope. Self-conditioned fields for large-eddy simulations of turbulent flows. J. Fluid Mech., Vol. 652, pp.139–169, 2010.
7. S.B. Pope. Turbulent flows. Cambridge University press, 2000.
8. S. B. Pope. Ten questions concerning the large-eddy simulation of turbulent flows. New Journal of Physics 35, 16 March 2004.
9. N. Soulopoulos. Experimental investigation of scalar mixing in unsteady turbulent jets. PhD thesis, University of London April 2009.
10. C. Tong, J. Wyngaard and J. Brasseurs. Experimental Study of the Subgrid-Scale Stresses in the Atmospheric Surface Layer. J. of Atmospheric sciences, Vol. 56. 15 July 1999.
11. C. Tong. Measurements of conserved scalar filtered density function in a turbulent jet. Physics of Fluids, Vol. 13, No. 10, October 2001.
12. C. Tong. Measurements of conserved scalar filtered density function in a turbulent jet. Physics of Fluids, Vol. 13, No. 10, October 2001.